




Article

Uroxite and metauroxite, the first two uranyl oxalate minerals

Anthony R. Kampf^{1*} , Jakub Plášil², Barbara P. Nash³, Ivan Němec⁴ and Joe Marty⁵

¹Mineral Sciences Department, Natural History Museum of Los Angeles County, 900 Exposition Boulevard, Los Angeles, CA 90007, USA; ²Institute of Physics ASCR, v.v.i., Na Slovance 1999/2, 18221 Prague 8, Czech Republic; ³Department of Geology and Geophysics, University of Utah, Salt Lake City, Utah 84112, USA;

⁴Department of Inorganic Chemistry, Faculty of Science, Charles University, Hlavova 8, 128 43 Prague 2, Czech Republic; and ⁵199 East Silver Oak Road, Salt Lake City, UT 84108, USA

Abstract

Uroxite (IMA2018-100), $[(\text{UO}_2)_2(\text{C}_2\text{O}_4)(\text{OH})_2(\text{H}_2\text{O})_2] \cdot \text{H}_2\text{O}$, and metauroxite (IMA2019-030), $(\text{UO}_2)_2(\text{C}_2\text{O}_4)(\text{OH})_2(\text{H}_2\text{O})_2$, are the first two uranyl oxalate minerals. Uroxite was found in the Markey mine, Red Canyon, San Juan County, Utah, USA and in the Burro mine, Slick Rock district, San Miguel County, Colorado, USA. Metauroxite was found only in the Burro mine. Both minerals are post-mining secondary phases found in efflorescent crusts on mine walls. Uroxite occurs as light yellow striated blades exhibiting moderate neon-green fluorescence, *ca* 2 Mohs hardness with good {101} and {010} cleavages. Calculated density = 4.187 g/cm³. Optics are: biaxial (–), $\alpha = 1.602(2)$, $\beta = 1.660(2)$, $\gamma = 1.680(2)$ (white light), $2V_{\text{meas.}} = 59(1)^\circ$, $2V_{\text{calc.}} = 59.1^\circ$, moderate $r > v$ dispersion, orientation $Y = \mathbf{b}$, $Z \wedge \mathbf{a} = 35^\circ$ in obtuse β and it is nonpleochroic. Metauroxite occurs as light yellow crude blades and tablets exhibiting weak green–grey fluorescence, *ca* 2 Mohs hardness with good {001} cleavage. Calculated density = 4.403 g/cm³. Approximate optics are: $\alpha' = 1.615(5)$ and $\gamma' = 1.685(5)$. Electron probe microanalysis provided UO_3 79.60, C_2O_3 10.02, H_2O 10.03, total 99.65 wt.% for uroxite and UO_3 82.66, C_2O_3 10.40, H_2O 7.81, total 100.87 wt.% for metauroxite; C_2O_3 and H_2O are based on the structures. Uroxite is monoclinic, $P2_1/c$, $a = 5.5698(2)$, $b = 15.2877(6)$, $c = 13.3724(9)$ Å, $\beta = 94.015(7)^\circ$, $V = 1135.86(10)$ Å³ and $Z = 4$. Metauroxite is triclinic, $P\bar{1}$, $a = 5.5635(3)$, $b = 6.1152(4)$, $c = 7.8283(4)$ Å, $\alpha = 85.572(5)$, $\beta = 89.340(4)$, $\gamma = 82.468^\circ$, $V = 263.25(3)$ Å³ and $Z = 1$. The strongest reflections of the powder XRD pattern [d , Å (I , %)(hkl)] are for uroxite: 10.05(38)(011), 5.00(100)(022, $\bar{1}11$), 4.75(23)(031), 4.43(51)(120, $\bar{1}02$), 3.567(33)(131), 3.341(29)(033, $\bar{1}32$, 004), 2.623(28)($\bar{2}02$, 015, $\bar{1}43$, 220) and for metauroxite: 6.06(45)(010), 5.52(33)(100), 4.97(34)(011), 4.52(100)($0\bar{1}1$, 101), 3.888(80)(111, 002, $\bar{1}10$), 3.180(51)($\bar{1}02$, $0\bar{1}2$), 2.604(32)($\bar{2}01$, $\bar{1}21$). In the structure of uroxite ($R_1 = 0.0333$ for 2081 $I > 2\sigma I$ reflections), UO_7 pentagonal bipyramids share corners forming $[\text{U}_4\text{O}_{24}]$ tetramers, which are linked by C_2O_4 groups to form corrugated sheets. In the structure of metauroxite ($R_1 = 0.0648$ for 1602 $I > 2\sigma I$ reflections) UO_7 pentagonal bipyramids share edges forming $[\text{U}_2\text{O}_{12}]$ dimers, which are linked by C_2O_4 groups to form zigzag chains.

Keywords: uroxite, metauroxite, new mineral, uranyl oxalate, crystal structure, Burro mine, Colorado, USA, Markey mine, Utah, USA

(Received 22 July 2019; accepted 26 August 2019; Accepted Manuscript published online: 02 September 2019; Associate Editor: Peter Leverett)

Introduction

The first synthetic uranium oxalates were reported in 1842 by Eugène-Melchior Péligot (e.g. Péligot, 1842). From these, he was able to show that the material that Martin Heinrich Klaproth discovered and named ‘urane’ in 1789 was actually an oxide, rather than a pure element. Péligot obtained green and yellow uranium oxalates by adding oxalic acid to uranium chloride in aqueous solution. He proposed the name ‘uranium’ for the metallic element and ‘uranyl’ for the yellow salts of uranium. As early as 1930, synthetic uranyl oxalate was being used in chemical actinometers. Today, actinide oxalates have important applications (Abraham *et al.*, 2014), particularly in the separation reprocessing of spent nuclear fuel, because of the chelating ability of the oxalate group with actinides. In the last several decades,

there have been numerous synthetic and structural studies of uranyl oxalates because of the unusual array of linking geometries that they demonstrate (Abraham *et al.*, 2014; Giesting *et al.*, 2006; Loiseau *et al.*, 2014); however, until now, uranyl oxalates have not been found in Nature.

Herein, we describe the first two uranyl oxalate minerals, uroxite and metauroxite. The name ‘uroxite’ is based on the mineral being a uranyl (UR) oxalate (OX). The name ‘metauroxite’ is based on the compositional similarity of the mineral to uroxite, with one less H_2O group per formula unit (pfu). These minerals correspond to known synthetic phases and both were reported with their structures by Duvieubourg *et al.* (2005). The new minerals and their names were approved by the Commission on New Minerals, Nomenclature and Classification of the International Mineralogical Association based upon proposals IMA2018-100 (Kampf *et al.*, 2018) for uroxite and 2019-030 (Kampf *et al.*, 2019) for metauroxite. The type specimens, all micromounts, have been deposited in the collections of the Natural History Museum of Los Angeles County, 900 Exposition Boulevard, Los Angeles, CA 90007, USA. Four uroxite

*Author for correspondence: Anthony R. Kampf, Email: akampf@nhm.org

Cite this article: Kampf A.R., Plášil J., Nash B.P., Němec I. and Marty J. (2020) Uroxite and metauroxite, the first two uranyl oxalate minerals. *Mineralogical Magazine* 84, 131–141. <https://doi.org/10.1180/mgm.2019.57>

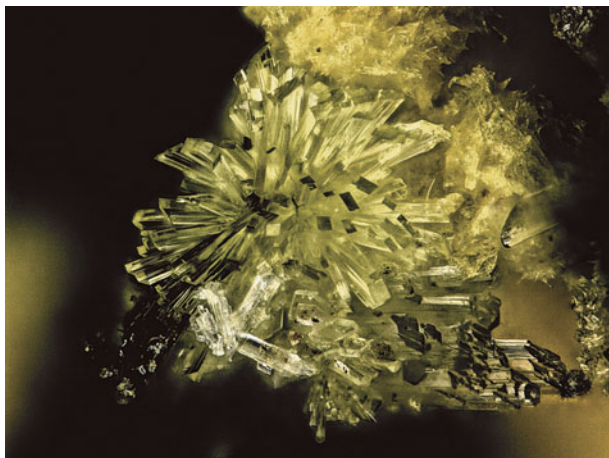


Fig. 1. Uroxite crystals from the Burro mine (cotype #73514). The field of view is 0.68 mm across.

cotypes are assigned catalogue numbers 73514 (Burro), 73515 (Burro), 73516 (Markey) and 73517 (Markey). Two metauroxite cotypes are assigned catalogue numbers 67289 and 67290.

Occurrence

Uroxite and metauroxite were first collected on September 22, 2016 underground in the Burro mine, Slick Rock district, San Miguel County, Colorado, USA (38°2'42"N, 108°53'23"W). Uroxite was collected on the following day, underground in the Markey mine, Red Canyon, White Canyon mining district, San Juan County, Utah (37°32'57"N, 110°18'08"W).

The Burro mine is near the southern end of the Uruan Mineral Belt, in which uranium and vanadium minerals occur together in bedded or roll-front deposits in the sandstone of the Salt Wash member of the Jurassic Morrison Formation (Carter and Gualtieri, 1965; Shawe, 2011). The uranium and vanadium ore mineralisation was deposited where solutions rich in U and V encountered pockets of strongly reducing solutions that had developed around accumulations of carbonaceous plant material. Mining operations have exposed both unoxidised and oxidised U and V phases. Under ambient temperatures and generally oxidising near-surface conditions, water reacts with pyrite to form aqueous solutions with relatively low pH, which then react with the earlier-formed phases, resulting in diverse suites of secondary minerals.

The Markey mine is located ~1 km southwest of the Blue Lizard mine, on the east-facing side of Red Canyon, ~72 km west of the town of Blanding, Utah, and ~22 km southeast of Good Hope Bay on Lake Powell. The geology of the Markey mine is quite similar to that of the Blue Lizard mine (Chenoweth, 1993; Kampf, *et al.*, 2017), although the secondary mineralogy of the Markey mine is notably richer in carbonate phases. The information following is taken largely from Chenoweth (1993). Mineralised channels are in the Shinarump member of the Chinle Formation. The Shinarump member consists of medium- to coarse-grained sandstone, conglomeratic sandstone beds and thick siltstone lenses. Ore minerals were deposited as replacements of wood and other organic material and as disseminations in the enclosing sandstone (Chenoweth, 1993). Since the mine closed in 1978, oxidation of primary ores in the humid underground environment has produced a variety

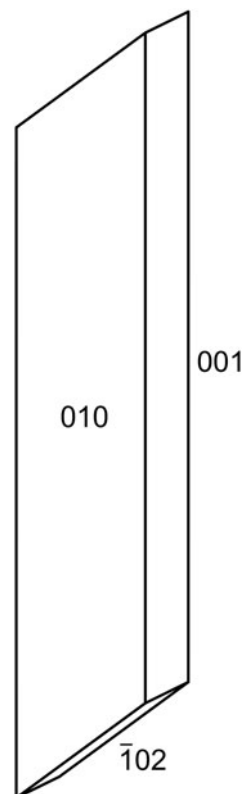


Fig. 2. Crystal drawing of uroxite crystal; clinographic projection.

of secondary minerals, mainly sulfates, as efflorescent crusts on the surfaces of mine walls (Kampf, *et al.*, 2017).

Uroxite and metauroxite are both rare and occur on asphaltum–quartz matrix. At the Markey mine, uroxite is associated with feynmanite and gypsum. At the Burro mine, both minerals are associated with abernathyite, gypsum, tyuyamunite, uranopilite and one other unidentified uranyl oxalate. At both the Burro and Markey mines, the oxalate presumably derives from the decomposed/fossilised organic matter noted above, most likely directly from the asphaltum on which the new minerals have formed.

Physical and optical properties

Uroxite

Uroxite occurs in radiating sprays of striated prisms or blades, up to ~1 mm long, elongate and striated on [100], more or less flattened on {010} and with steeply sloping terminations (Figs 1 and 2). The prism forms are {010} and {001} and the termination is { $\bar{1}02$ }. The colour is light yellow, the lustre is vitreous and the streak is very pale yellow. Crystals are brittle, with Mohs hardness of *ca* 2, uneven fracture, one perfect cleavage on { $\bar{1}02$ } and one fair cleavage on {001}. Moderate neon-green fluorescence is observed under 405 nm laser illumination. The density could not be measured with available density liquids; uroxite appears to gradually dissolve in Clerici solution. The calculated density is 4.187 g cm⁻³ for both the empirical and ideal formulas. Uroxite is optically biaxial (–) with $\alpha = 1.602(2)$, $\beta = 1.660(2)$ and $\gamma = 1.680(2)$, determined in white light. The 2V measured directly on a spindle stage is 59(1)°; the calculated 2V is 59.1°. There is

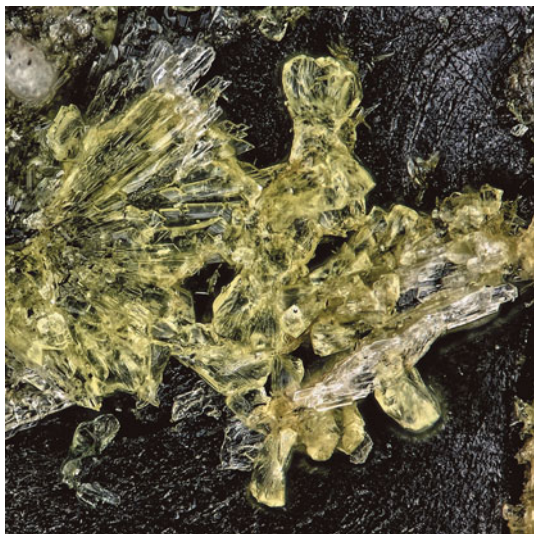


Fig. 3. Yellow, bowtie-like intergrowths of metauroxite crystals (right-centre), yellow radiating uroxite prisms (left) and colourless gypsum blades on asphaltum matrix (cotype #67289). The field of view is 0.50 mm across.

moderate $r > v$ dispersion. The optical orientation is $Y = \mathbf{b}$ and $Z \wedge \mathbf{a} = 35^\circ$ in obtuse β . No pleochroism was observed. The Gladstone–Dale compatibility, $1 - (K_p/K_c)$, is 0.005, in the

superior range (Mandarino, 1981) for both the empirical and ideal formulas. At room temperature, uroxite is insoluble in H_2O and slowly soluble in dilute HCl.

Metauroxite

Metauroxite occurs as crude blades and lozenge-shaped tablets, up to $\sim 100 \mu\text{m}$ in maximum dimension; commonly in irregular and bowtie-like intergrowths to $\sim 200 \mu\text{m}$ across (Fig. 3). No crystal forms could be measured because faces are generally poorly formed; the tablets are apparently flattened on $\{011\}$. Twinning is ubiquitous, by 180° rotation around the perpendicular to $\{011\}$ (indicated by single-crystal diffraction data); observation of crystals under crossed polars suggests that the twinning is commonly polysynthetic. The colour is light yellow, the lustre is vitreous and the streak is very pale yellow. Crystals are brittle, with Mohs hardness of *ca* 2, uneven fracture and two good cleavages probably on $\{101\}$ and $\{010\}$ on the basis of the structure. Weak green–grey fluorescence is observed under 405 nm laser illumination. The density could not be measured with available density liquids. The calculated density is 4.403 g cm^{-3} for both the empirical and ideal formulas. Optical determinations were problematic because of poor crystal quality and polysynthetic twinning. It was only possible to obtain approximate minimum (α') and maximum (γ') indices of refraction: $\alpha' = 1.615(5)$ and $\gamma' = 1.685(5)$ measured in white light. The average of the estimated minimum and maximum indices of refraction is 1.65,

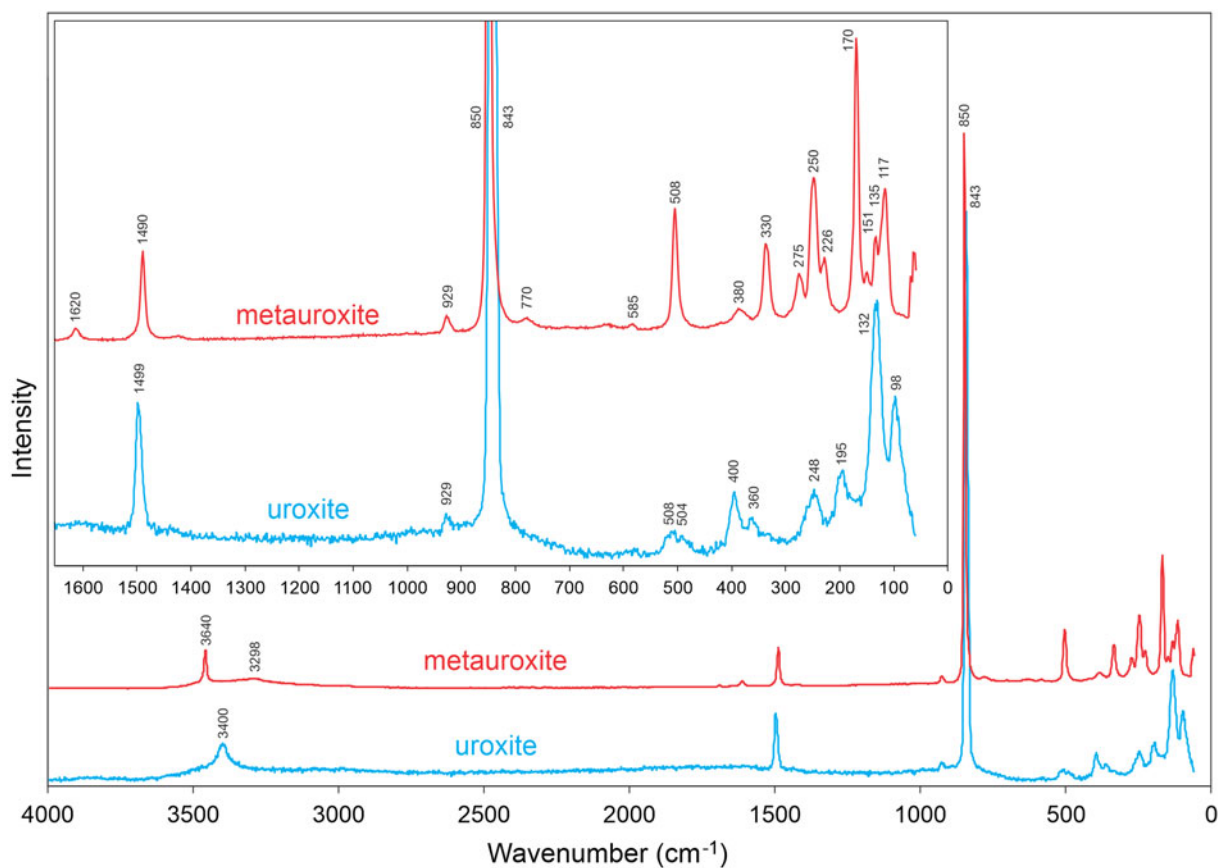


Fig. 4. Raman spectra of uroxite and metauroxite recorded using a 532 nm diode laser. The inset shows the expanded $1650\text{--}0 \text{ cm}^{-1}$ region. Note that the uroxite spectrum had to be recorded at much lower laser intensity and has been scaled by $\times 6$ relative to that of metauroxite, which accounts for the lower signal-to-noise ratio for the uroxite spectrum.

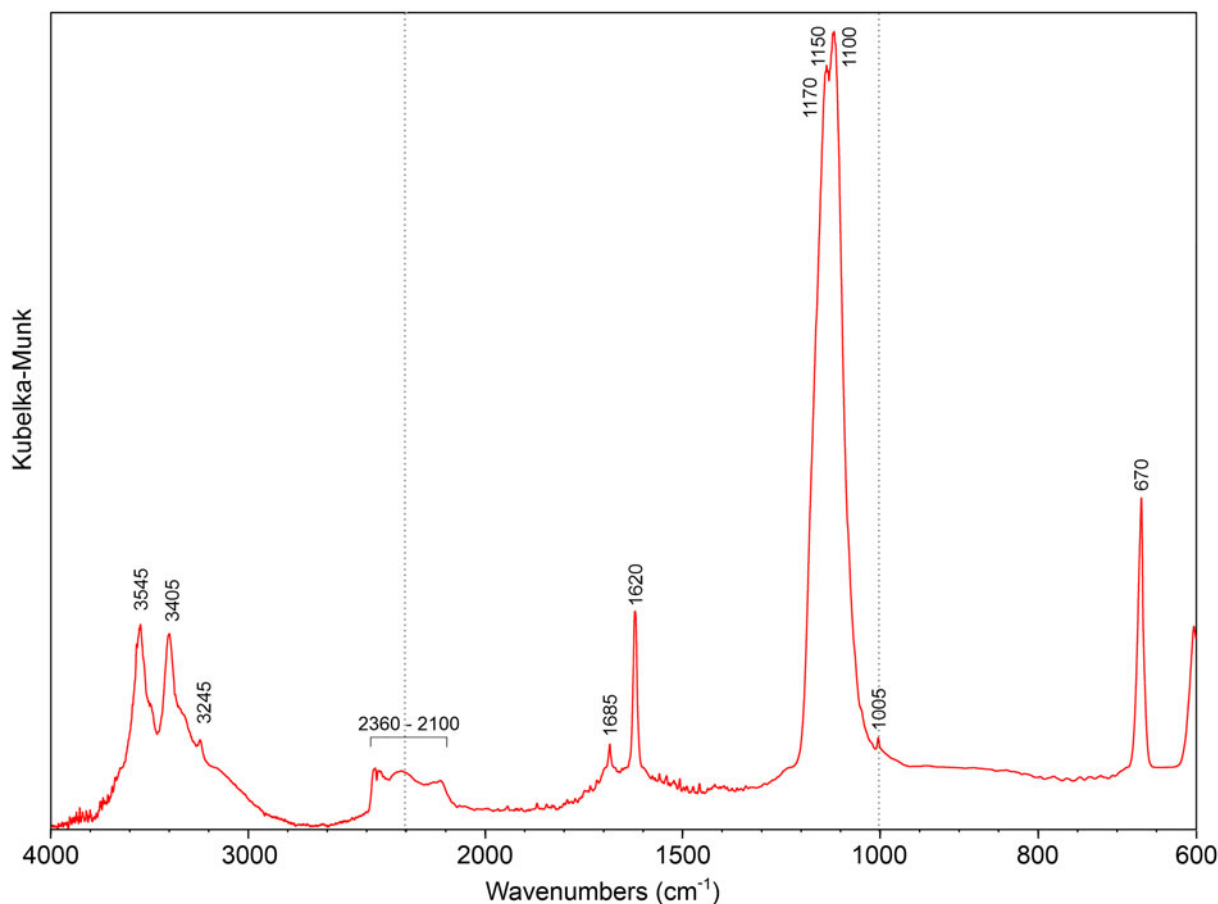


Fig. 5. Infrared spectrum (micro-DRIFTS) of uroxite. Note changes in horizontal scale at dotted lines.

Table 1. Band assignments for the Raman and infrared spectra of uroxite and metauroxite.

Uroxite		Metauroxite		Assignment
Infrared	Raman	Raman	Raman	
3545, 3405, 3245	3400	3640	3298	$\nu(\text{O-H})$ stretching of OH^- $\nu(\text{O-H})$ stretching of H_2O overtone ($2 \times 1150 \text{ cm}^{-1}$)
2360–2100				
1685		1620		$\nu_2(\delta)$ (H–O–H) bending
1620				$\nu_8(\text{as}, B_{2u})$ (C–O) asymmetric stretching
	1499	1490		$\nu_1(A_g)$ (C–O) symmetric stretching
1170, 1150, 1100				$\nu_5(B_{1u})$ (C–O) asymmetric stretching
	929	929		$\nu_3(\text{UO}_2)^{2+}$ asymmetric stretching
1005				unassigned
	843	850		$\nu_1(\text{UO}_2)^{2+}$ symmetric stretching
		770		H_2O libration
670				$\nu_6(B_{1u})$ (δ)(O–C–O) asymmetric bending
		585		$\nu(\text{U-O}_{\text{eq}})$ and $\nu(\text{U-OH})$ stretching; or H_2O libration
	508, 504	508		$\nu_3(A_g)$ (δ)(O–C–O) symmetric bending
	400, 360	380		four possibilities: $\gamma(\text{U}(\text{OH})\text{--U})$, $\nu(\text{U}(\text{OH}))$, H_2O libration, $\nu_7(\rho_{w,s}/\omega_s)$ (O–C–O) rocking
		330		$\nu(\text{U}(\text{OH}))$ or H_2O libration
	248	275, 250, 226		$\nu_2(\delta)$ (O–U–O) and/or (δ)(U–OH)–U bending
	132	135		$\nu_4(\tau)$ (C–C) torsion
	195, 98	170, 151, 117		phonons

Table 2. Chemical compositions (in wt.%) for uroxite and metauroxite.

Constituent	Uroxite	Metauroxite
UO ₃	79.60 (78.04–81.90)	82.66 (82.13–82.96)
C ₂ O ₃ *	10.02	10.40
H ₂ O*	10.03	7.81
Total	99.65	100.87

* Based on the structure.

which gives a Gladstone-Dale compatibility, $1 - (K_p/K_c)$, of 0.0195, in the superior range (Mandarino, 1981) for the empirical formula. At room temperature, metauroxite is insoluble in H₂O and slowly soluble in dilute HCl.

Raman and infrared spectroscopy

Raman spectra for both minerals were recorded from 4000 to 60 cm⁻¹ using a 532 nm diode laser on a Horiba XploRA PLUS. Uroxite suffered quick decomposition at laser power >1%; however, metauroxite was less susceptible to decomposition, perhaps because its structure does not include an isolated H₂O group (see below). The uroxite spectrum was recorded at 1% power and that of metauroxite was recorded at 10% power. The intensity of the uroxite spectrum shown in Fig. 4 was factored by ×6 relative to that of metauroxite.

Relatively large crystals of uroxite enabled us to perform micro-diffuse reflectance infrared Fourier transform spectroscopy (micro-DRIFTS) using a Thermo Nicolet 6700 FTIR spectrometer

Table 3. Powder X-ray diffraction data (*d* in Å) for uroxite*.

<i>l</i> _{obs}	<i>l</i> _{calc}	<i>d</i> _{obs}	<i>d</i> _{calc}	<i>h k l</i>
38	38	10.05	10.0512	011
7	7	6.64	6.6322	021
9	9	6.11	6.1133	012
8	9	5.55	5.5561	100
100	51, 49	5.00	5.0256, 4.9750	022, 111
23	22	4.75	4.7604	031
51	14, 35	4.43	4.4943, 4.4240	120, 102
	4		4.3340	121
13	4, 7	4.015	4.0493, 3.9863	032, 112
16	12	3.844	3.8435	023
8	7	3.739	3.7555	130
19	12, 8	3.649	3.6741, 3.6330	041, 122
33	31	3.567	3.5712	131
	3		3.5011	113
29	17, 4, 5	3.341	3.3504, 3.3407, 3.3349	033, 132, 004
	5		3.3161	042
20	12, 8	3.271	3.2806, 3.2583	113, 014
12	10	3.070	3.0750	123
	3		3.0378	141
5	6	2.975	2.9803	051
9	9	2.933	2.9385	133
	3		2.8985	114
8	4	2.754	2.7538	124
	4		2.7303	114
9	9	2.672	2.6787	150
	6		2.6436	151
28	5, 7, 7, 10	2.623	2.6307, 2.6282, 2.6193, 2.6110	202, 015, 143, 220
10	4, 5	2.515	2.5311, 2.5031	221, 202
12	6, 7	2.433	2.4370, 2.4259	134, 231
5	5	2.385	2.4036	213
	3		2.3534	125
10	6	2.334	2.3376	232
8	5	2.253	2.2610	153
16	8, 3, 6	2.201	2.2107, 2.2079, 2.1876	063, 162, 045
5	3	2.117	2.1248	224
12	4	2.0516	2.0548	154
13	5, 4, 6	2.0286	2.0378, 2.0300, 2.0160	036, 163, 106
20	4, 9	1.9985	1.9987, 1.9968	116, 145
10	8	1.9583	1.9614	243
11	8, 3	1.9216	1.9306, 1.9110	172, 080
5	3, 4	1.8919	1.9042, 1.8910	253, 017
13	3, 5	1.8468	1.8580, 1.8474	235, 261
14	5, 4, 3, 4, 3	1.8075	1.8270, 1.8075, 1.8045, 1.7981, 1.7922	074, 225, 311, 056, 254
12	5, 6	1.7764	1.7748, 1.7683	165, 322
10	3, 3, 4	1.7494	1.7557, 1.7543, 1.7408	174, 182, 331
7	4, 4	1.6669	1.6695, 1.6598	304, 147
7	3	1.6557	1.6576	018
4	3	1.6241	1.6165	191
6	3	1.5213	1.5209	352
10	3	1.4532	1.4553	345

*The calculated intensities have been scaled such that the intensities of the adjacent 022 and 111 lines total 100. After scaling, only calculated lines with *l* ≥ 3 are included. Further data are in the Supplementary material. The strongest lines are given in bold.

Table 4. Powder X-ray diffraction data (d in Å) for metauroxite.

l_{obs}	l_{calc}	d_{obs}	d_{calc}	hkl
9	10	7.90	7.8016	001
45	61	6.06	6.0432	010
33	38	5.52	5.5148	100
34	55	4.97	4.9665	011
100	24, 76	4.52	4.6087, 4.5031	011, 101
	6		4.3724	110
80	44, 25, 34	3.888	3.9081, 3.9008, 3.8287	111, 002, 110
22	32	3.748	3.7267	$\bar{1}\bar{1}\bar{1}$
	5		3.5056	$\bar{1}\bar{1}\bar{1}$
51	36, 20	3.180	3.1848, 3.1680	102, 012
7	4, 7	2.999	3.0216, 2.9948	020, 112
7	12	2.888	2.8938	021
	2		2.8335	$\bar{1}\bar{1}\bar{2}$
15	7, 12	2.796	2.8116, 2.8018	120, $\bar{1}\bar{1}\bar{2}$
14	19	2.746	2.7473	021
	5		2.6680	$\bar{1}\bar{1}\bar{2}$
	7		2.6445	210
32	24, 8	2.604	2.5999, 2.5866	201, 121
	5		2.5133	$\bar{1}\bar{2}\bar{0}$
	4		2.4832	022
	4		2.4793	$\bar{2}\bar{1}\bar{1}$
22	8, 16	2.455	2.4586, 2.4383	013, $\bar{1}\bar{2}\bar{1}$
	3		2.3917	$\bar{2}\bar{1}\bar{0}$
20	6, 6, 9	2.352	2.3626, 2.3520, 2.3486	122, 103, $\bar{1}\bar{2}\bar{1}$
	3		2.3066	$\bar{2}\bar{1}\bar{1}$
	3		2.3043	022
13	5, 8	2.2611	2.2673, 2.2518	$\bar{2}\bar{1}\bar{1}$, $\bar{2}\bar{0}\bar{2}$
27	18, 3, 9	2.2136	2.2239, 2.2071, 2.2019	212, $\bar{1}\bar{2}\bar{2}$, $\bar{1}\bar{1}\bar{3}$
11	4, 10, 3	2.1683	2.1862, 2.1823, 2.1555	220, $\bar{1}\bar{1}\bar{3}$, $\bar{2}\bar{1}\bar{2}$
	3		2.1362	221
	4		2.1039	$\bar{1}\bar{1}\bar{3}$
16	10, 5	2.0664	2.0674, 2.0536	$\bar{2}\bar{1}\bar{2}$, $\bar{1}\bar{2}\bar{2}$
8	10	2.0107	2.0144	030
	4		1.9785	130
9	7, 2	1.9510	1.9534, 1.9504	131, 004
18	8, 7, 5	1.8994	1.9144, 1.9000, 1.8920	$\bar{2}\bar{2}\bar{0}$, $\bar{0}\bar{2}\bar{3}$, $\bar{2}\bar{0}\bar{3}$
	6, 5		1.8681, 1.8634	$\bar{1}\bar{2}\bar{3}$, $\bar{2}\bar{2}\bar{2}$
22	5, 8, 8	1.8454	1.8489, 1.8444, 1.8389	032, $\bar{1}\bar{2}\bar{3}$, $\bar{1}\bar{0}\bar{4}$
21	5, 5, 6, 6, 4	1.8171	1.8274, 1.8238, 1.8193, 1.8157, 1.7967	310, $\bar{2}\bar{1}\bar{3}$, 114, $\bar{0}\bar{1}\bar{4}$, $\bar{1}\bar{3}\bar{1}$
	4		1.7893	301
	2		1.7885	311
17	3, 2, 5, 2, 4	1.7382	1.7528, 1.7454, 1.7423, 1.7361, 1.7342	$\bar{2}\bar{2}\bar{2}$, $\bar{1}\bar{1}\bar{4}$, $\bar{1}\bar{3}\bar{1}$, $\bar{0}\bar{3}\bar{2}$, $\bar{2}\bar{1}\bar{3}$
13	4, 4, 5, 4, 2, 4	1.7073	1.7230, 1.7213, 1.7130, 1.6994, 1.6921, 1.6863	231, 223, $\bar{1}\bar{3}\bar{2}$, 024, $\bar{1}\bar{3}\bar{2}$, $\bar{2}\bar{2}\bar{2}$
16	3, 2, 3, 4, 2	1.6652	1.6749, 1.6698, 1.6659, 1.6628, 1.6592	$\bar{2}\bar{3}\bar{1}$, 312, $\bar{3}\bar{1}\bar{1}$, 302, 124
	4		1.6510	$\bar{3}\bar{1}\bar{1}$
11	4, 3, 4	1.6401	1.6493, 1.6403, 1.6354	321, $\bar{3}\bar{1}\bar{2}$, 133
	3		1.6208	$\bar{3}\bar{2}\bar{1}$
	2		1.5955	214
12	7, 2, 3	1.5885	1.5923, 1.5840, 1.5790	204, $\bar{0}\bar{2}\bar{4}$, $\bar{2}\bar{2}\bar{3}$
	2		1.5603	005
8	2, 2, 2, 3	1.5399	1.5513, 1.5362, 1.5347, 1.5209	$\bar{2}\bar{3}\bar{2}$, $\bar{0}\bar{3}\bar{3}$, $\bar{2}\bar{1}\bar{4}$, $\bar{2}\bar{3}\bar{1}$
16	3, 2, 3, 5, 2, 2	1.5012	1.5118, 1.5108, 1.5032, 1.5013, 1.4951, 1.4929	313, 040, 141, 105, $\bar{1}\bar{2}\bar{4}$, 233

* The calculated intensities have been scaled such that the intensities of the adjacent $0\bar{1}\bar{1}$ and 101 lines total 100. After scaling, only calculated lines with $I \geq 2$ are included. The strongest lines are given in bold.

(range 4000–600 cm^{-1} , resolution 4 cm^{-1} , 128 scans, Happ-Genzel apodisation) equipped with a Spectra Tech InspectIR Plus micro-spectroscopic accessory (liquid N_2 cooled Hg–Cd–Te detector). Uroxite crystals were pulverised, mixed with KBr and analysed immediately without preparation of the pellet. Pure KBr was taken as the blank reference. The infrared spectrum for uroxite is shown in Fig. 5.

The band assignments for the infrared and Raman spectra shown in Table 1 are based on papers by Bartlett and Cooney (1989), Čejka (1999), Colmenero (2019), Mancilla *et al.* (2009), Peterson and Pullman (2016) and Shippey (1980). According to the correlation given by Libowitzky (1999), the bands in the spectra attributed to ν (O–H) correspond to hydrogen bonds ranging

from ~ 3.2 to 2.8 Å. Bartlett and Cooney (1989) provided an empirical relationship to derive the approximate U–O_{Ur} bond lengths from the band position assigned to the ν_1 (UO_2)²⁺ stretching vibration, which gives 1.77 Å for uroxite and 1.76 Å for metauroxite, in excellent agreement with U–O_{Ur} bond lengths from the X-ray data: 1.763 and 1.767 Å for uroxite and 1.775 Å for metauroxite.

Chemical composition

Chemical analyses were performed at the University of Utah on a Cameca SX-50 electron microprobe with four wavelength dispersive spectrometers and using *Probe for EPMA* software. Analytical

Table 5. Data collection and structure refinement details for uroxite and metauroxite.

	Uroxite	Metauroxite
Diffractometer	Rigaku R-Axis Rapid II	Rigaku R-Axis Rapid II
X-ray radiation/power	MoK α ($\lambda = 0.71075 \text{ \AA}$)	MoK α ($\lambda = 0.71075 \text{ \AA}$)
X-ray power	50 kV, 40 mA	50 kV, 40 mA
Temperature (K)	293(2)	293(2) K
Structural formula	$[(\text{UO}_2)_2(\text{C}_2\text{O}_4)(\text{OH})_2(\text{H}_2\text{O})_2] \cdot \text{H}_2\text{O}$	$(\text{UO}_2)_2(\text{C}_2\text{O}_4)(\text{OH})_2(\text{H}_2\text{O})_2$
Refined formula	$\text{U}_2 \text{ C}_2 \text{ H}_8 \text{ O}_{13}$	$\text{U}_2 \text{ C}_2 \text{ O}_{12}$
Crystal system, space group	Monoclinic, $P2_1/c$	Triclinic, $P\bar{1}$
Unit-cell dimensions	$a = 5.5698(2) \text{ \AA}$ $b = 15.2877(6) \text{ \AA}$ $c = 13.3724(9) \text{ \AA}$ $\beta = 94.015(7)^\circ$	$a = 5.5635(3) \text{ \AA}$ $b = 6.1152(4) \text{ \AA}$ $c = 7.8283(4) \text{ \AA}$ $\alpha = 85.572(5)^\circ$ $\beta = 89.340(4)^\circ$ $\gamma = 82.468(5)^\circ$
$V (\text{\AA}^3)$	1135.87(10)	263.25(3)
Z	4	1
Density (refined formula, g cm^{-3})	4.118	4.366
Absorption coefficient (mm^{-1})	28.542	30.775
$F(000)$	1232	292
Crystal size (μm)	$80 \times 30 \times 30$	$30 \times 30 \times 20$
θ range ($^\circ$)	3.05 to 25.02	2.61 to 25.05
Index ranges	$-6 \leq h \leq 7$ $-8 \leq k \leq 18$ $-15 \leq l \leq 15$	$-6 \leq h \leq 6$ $-6 \leq k \leq 7$ $-9 \leq l \leq 9$
Refl. collected/unique	12103/1995; $R_{\text{int}} = 0.054$	6484/1700; $R_{\text{int}} = 0.0704$
Refl. with $I > 2\sigma$	1777	1602
Completeness to θ max	99.8%	99.1%
Refinement method	Full-matrix least-squares on F^2	Full-matrix least-squares on F^2
Parameter/restraints	178/11	74/0
GoF	1.071	1.146
Final R indices [$I > 2\sigma$]	$R_1 = 0.0253$, $wR_2 = 0.0511$	$R_1 = 0.0648$, $wR_2 = 0.1830$
R indices (all data)	$R_1 = 0.0308$, $wR_2 = 0.0531$	$R_1 = 0.0683$, $wR_2 = 0.1849$
Largest diff. peak/hole ($e^- \text{ \AA}^{-3}$)	+1.14/−0.90	+3.30/−2.65
Twin matrix	–	0.272 0.196 −0.729 0.001 −1.000 −0.001 −1.270 −0.196 −0.272
Twin fractions	–	0.453/0.547

$R_{\text{int}} = \sum |F_o^2 - F_c^2(\text{mean})| / \sum F_o^2$. $\text{GoF} = S = \{ \sum [w(F_o^2 - F_c^2)^2] / (n-p) \}^{1/2}$. $R_1 = \sum |F_o| - |F_c| / \sum F_o$. $wR_2 = \{ \sum [w(F_o^2 - F_c^2)^2] / \sum [w(F_o^2)^2] \}^{1/2}$; $w = 1 / [\sigma^2(F_o^2) + (aP)^2 + bP]$ and P is $[2F_c^2 + \text{Max}(F_o, 0)]/3$; for uroxite a is 0.0169 and b is 6.577; for metauroxite a is 0.0746 and b is 28.4245.

Table 6. Atom coordinates and displacement parameters (\AA^2) for uroxite.

	x/a	y/b	z/c	U_{eq}	U^{11}	U^{22}	U^{33}	U^{23}	U^{13}	U^{12}
U1	0.21995(5)	0.46057(2)	0.28584(2)	0.01947(10)	0.01833(18)	0.01818(17)	0.0216(2)	−0.00236(12)	−0.00050(13)	−0.00055(11)
U2	0.53127(5)	0.18517(2)	0.04232(2)	0.01866(10)	0.01823(17)	0.01727(17)	0.02025(19)	−0.00089(12)	−0.00033(13)	−0.00030(11)
C1	0.8707(14)	0.3512(5)	0.1192(7)	0.0244(19)	0.022(4)	0.025(5)	0.027(5)	−0.001(4)	0.006(4)	0.003(4)
C2	0.8959(13)	0.2888(5)	0.2060(6)	0.0194(18)	0.010(4)	0.030(5)	0.018(5)	−0.001(3)	−0.002(3)	0.007(3)
O1	0.7406(10)	0.3287(3)	0.0432(5)	0.0297(14)	0.039(4)	0.022(3)	0.027(4)	0.000(3)	−0.009(3)	−0.011(3)
O2	0.9836(10)	0.4233(3)	0.1295(5)	0.0290(14)	0.033(3)	0.021(3)	0.032(4)	0.000(2)	−0.008(3)	−0.011(3)
O3	0.7848(10)	0.2178(3)	0.1970(4)	0.0262(14)	0.030(3)	0.016(3)	0.032(4)	−0.001(2)	−0.003(3)	−0.005(2)
O4	0.0279(10)	0.3128(3)	0.2817(4)	0.0252(13)	0.029(3)	0.022(3)	0.025(4)	0.002(2)	−0.003(3)	−0.003(2)
O5	0.9670(10)	0.5150(4)	0.3275(4)	0.0273(14)	0.025(3)	0.027(3)	0.029(4)	0.001(3)	−0.002(3)	0.002(2)
O6	0.4749(10)	0.4080(4)	0.2422(5)	0.0317(14)	0.033(3)	0.031(3)	0.032(4)	−0.010(3)	0.007(3)	−0.002(3)
O7	0.2879(10)	0.2312(4)	0.1011(5)	0.0323(15)	0.034(3)	0.030(3)	0.034(4)	−0.010(3)	0.005(3)	−0.003(3)
O8	0.7771(10)	0.1393(4)	0.9830(5)	0.0306(14)	0.022(3)	0.031(3)	0.039(4)	−0.004(3)	0.005(3)	0.002(2)
OH1	0.4801(9)	0.5628(3)	0.3569(4)	0.0232(13)	0.015(3)	0.023(3)	0.031(4)	−0.010(2)	0.002(3)	−0.002(2)
H1	0.638(7)	0.549(5)	0.338(7)	0.035						
OH2	0.2640(9)	0.1037(3)	0.9428(4)	0.0225(13)	0.018(3)	0.023(3)	0.026(4)	0.001(2)	0.000(2)	−0.004(2)
H2	0.135(11)	0.091(5)	0.984(5)	0.034						
OW1	0.3998(12)	0.2775(4)	0.8952(5)	0.0385(17)	0.053(4)	0.020(3)	0.040(5)	0.003(3)	−0.018(3)	−0.008(3)
H1a	0.365(13)	0.336(3)	0.914(6)	0.046						
H1b	0.270(11)	0.258(5)	0.850(6)	0.046						
OW2	0.2141(13)	0.5825(4)	0.1631(5)	0.0399(17)	0.063(5)	0.033(4)	0.025(4)	0.000(3)	0.006(3)	−0.016(3)
H2a	0.208(16)	0.635(3)	0.203(5)	0.048						
H2b	0.300(15)	0.597(5)	0.106(4)	0.048						
OW3	0.6771(15)	0.5578(5)	0.0483(7)	0.064(2)	0.080(6)	0.031(4)	0.078(7)	0.006(4)	−0.012(5)	0.017(4)
H3a	0.719(16)	0.498(3)	0.071(8)	0.077						
H3b	0.816(13)	0.577(6)	0.014(8)	0.077						

Table 7. Atom coordinates and displacement parameters (\AA^2) for metauroxite.

	x/a	y/b	z/c	U_{eq}	U^{11}	U^{22}	U^{33}	U^{23}	U^{13}	U^{12}
U1	0.3654(2)	0.3519(2)	0.20317(15)	0.0207(4)	0.0182(6)	0.0240(7)	0.0200(6)	-0.0014(4)	0.0004(4)	-0.0027(4)
C	0.023(6)	0.379(6)	0.545(4)	0.027(7)	0.025(17)	0.033(19)	0.026(17)	0.005(14)	-0.017(14)	-0.012(14)
O1	0.606(4)	0.416(4)	0.325(3)	0.028(5)	0.022(11)	0.051(15)	0.011(10)	0.004(10)	-0.008(8)	-0.001(10)
O2	0.131(5)	0.268(4)	0.077(4)	0.038(6)	0.032(13)	0.029(13)	0.055(16)	0.009(11)	-0.012(12)	-0.017(11)
O3	0.176(4)	0.244(4)	0.474(3)	0.028(5)	0.030(12)	0.016(11)	0.037(13)	-0.011(9)	0.013(10)	0.003(9)
O4	0.079(4)	0.650(4)	0.314(3)	0.032(5)	0.026(12)	0.030(13)	0.040(14)	-0.003(11)	0.015(11)	-0.010(10)
OH5	0.370(4)	0.688(4)	0.040(3)	0.028(5)	0.019(11)	0.036(14)	0.028(12)	-0.004(10)	0.011(9)	-0.002(10)
OW6	0.522(5)	-0.029(4)	0.254(3)	0.034(6)	0.045(15)	0.028(13)	0.026(12)	-0.001(10)	-0.008(11)	0.006(11)

conditions were 15 kV accelerating voltage, 10 nA beam current and beam diameters of 15 μm (for uroxite from the Burro mine) and 5 μm (for metauroxite). Counting times were 30 s on peak and 15 s on background. Raw X-ray intensities were corrected for matrix effects with a $\varphi\rho(z)$ algorithm (Pouchou and Pichoir, 1991); ideal formula concentrations of O and C were used for the matrix calculations. Synthetic UO_2 was used as the probe standard for UO_3 . A time-dependent intensity correction was applied for ingrowth of U. Because insufficient material is available for a direct determination of C_2O_3 or H_2O , they are calculated based upon the structure determination. For uroxite from Burro, eight points on four crystals were analysed and, for metauroxite, eight points on five crystals were analysed. The results are given in Table 2.

For uroxite, the empirical formula (calculated on the basis of 13 O atoms pfu) is $[(\text{U}_{1.00}\text{O}_2)_2(\text{C}_2\text{O}_4)(\text{OH})_2(\text{H}_2\text{O})_2]\cdot\text{H}_2\text{O}$ and the ideal formula is $[(\text{UO}_2)_2(\text{C}_2\text{O}_4)(\text{OH})_2(\text{H}_2\text{O})_2]\cdot\text{H}_2\text{O}$, which requires UO_3 79.88, C_2O_3 10.06, H_2O 10.06, total 100.00 wt.%.

For metauroxite, the empirical formula (calculated on the basis of 12 O atoms pfu) is $(\text{U}_{1.00}\text{O}_2)_2(\text{C}_2\text{O}_4)(\text{OH})_2(\text{H}_2\text{O})_2$. The ideal formula is $(\text{UO}_2)_2(\text{C}_2\text{O}_4)(\text{OH})_2(\text{H}_2\text{O})_2$, which requires UO_3 81.94, C_2O_3 10.32, H_2O 7.74, total 100.00 wt.%.

X-ray crystallography and structure refinement

Powder X-ray studies were done using a Rigaku R-Axis Rapid II curved imaging plate microdiffractometer, with monochromatised $\text{MoK}\alpha$ radiation ($\lambda = 0.71075 \text{ \AA}$). A Gandolfi-like motion on the φ and ω axes was used to randomise the samples and observed d

Table 8. Selected bond distances (\AA) for uroxite.

U1-O5	1.760(6)	U2-O7	1.760(6)	C1-C2	1.501(12)
U1-O6	1.766(6)	U2-O8	1.774(6)	C1-O1	1.254(10)
U1-OH1	2.292(5)	U2-OH2	2.294(5)	C1-O2	1.271(9)
U1-OH2	2.315(6)	U2-OH1	2.309(5)	C2-O3	1.252(9)
U1-OW2	2.458(6)	U2-O3	2.473(6)	C2-O4	1.263(9)
U1-O4	2.483(5)	U2-O1	2.485(5)	<C-O>	1.260
U1-O7	2.498(6)	U2-OW1	2.490(6)		
<U1-O _{U1} >	1.763	<U2-O _{U1} >	1.767		
<U1-O _{eq} >	2.409	<U2-O _{eq} >	2.410		

Hydrogen bonds

$D-H\cdots A$	$D-H$	$H\cdots A$	$D\cdots A$	$\angle D-H\cdots A$
OH1-H1 \cdots O5	0.96(2)	1.92(3)	2.863(8)	168(8)
OH2-H2 \cdots O8	0.96(2)	2.12(6)	2.854(8)	132(7)
OW1-H1a \cdots OW3	0.96(2)	1.71(2)	2.671(9)	176(7)
OW1-H1b \cdots O4	0.96(2)	1.91(3)	2.840(8)	164(7)
OW2-H2a \cdots O3	0.96(2)	1.84(3)	2.788(9)	168(8)
OW2-H2b \cdots O1	0.96(2)	2.29(6)	3.100(9)	142(8)
OW3-H3a \cdots O2	0.98(2)	1.99(6)	2.840(9)	144(8)
OW3-H3b \cdots O2	0.98(2)	2.28(7)	3.153(11)	148(10)

values and intensities were derived by profile fitting using *JADE 2010* software (Materials Data, Inc.). The powder data for uroxite (Table 3) and those for metauroxite (Table 4) show good agreement with the patterns calculated from the structure determinations.

For both minerals, the single-crystal structure data were collected at room temperature using the same diffractometer and radiation noted above. The Rigaku *CrystalClear* software package was used for processing the structure data, including the application of an empirical absorption correction using the multi-scan method with *ABSCOR* (Higashi, 2001). For uroxite, a single crystal from the Burro mine was used for the data collection. For metauroxite, the crystal used was twinned by 180° rotation around the perpendicular to {011}, as indicated by the *TwinSolve* program within the Rigaku *CrystalClear* software package. Initial structure models were obtained using *SIR2011* (Burla *et al.*, 2012). *SHELXL-2016* (Sheldrick, 2015) was used for the refinement of the structures.

For uroxite, difference-Fourier syntheses located all non-hydrogen atoms not located in the original structure solution, and subsequent cycles located all H sites. The structure was found to be identical to that of synthetic compound (#3 of Duvieubourg *et al.*, 2005), which lacks the positions of H atoms. The H atoms were refined with soft constraints of 0.97(2) \AA on the O-H distances and with the U_{eq} of each H set to 1.5 times that of the donor OH and 1.2 times that of the donor OW atom. For metauroxite, difference-Fourier syntheses failed to locate H atoms. The high residuals are attributed to the relatively poor crystal quality, to the difficulty in integrating the twinned reflections and to the inability of the *ABSCOR* program to completely correct for the absorption by the twinned crystal. The metauroxite structure was found to be identical to that of synthetic compound #1 of Duvieubourg *et al.* (2005). For both structures, data collection and refinement details are given in Table 5. Atom coordinates and displacement parameters for uroxite are in Table 6 and those for metauroxite in Table 7. Selected bond distances for uroxite are in Table 8 and those for metauroxite are in Table 9. A bond-valence analysis for uroxite is in Table 10 and that for metauroxite is in Table 11. The crystallographic information files have been deposited with the Principal Editor of

Table 9. Selected bond distances (\AA) for metauroxite.

U-O1	1.75(2)	C-C	1.58(6)	Hydrogen bonds ($D\cdots A$)	
U-O2	1.80(2)	C-O3	1.26(4)	OH5 \cdots O2	2.91(3)
U-OH5	2.34(2)	C-O4	1.25(4)	OW6 \cdots OH5	2.71(3)
U-OW6	2.38(2)			OW6 \cdots O3	2.85(3)
U-OH5	2.40(2)				
U-O3	2.44(2)				
U-O4	2.46(2)				
<U-O _{U1} >	1.775				
<U-O _{eq} >	2.404				

Table 10. Bond-valence analysis for uroxite. Values are expressed in valence units.*

	U1	U2	C1	C2	H1	H2	H1a	H1b	H2a	H2b	H3a	H3b	Σ
O1		0.40	1.43							0.14			1.97
O2	0.42		1.37								0.19	0.14	2.12
O3		0.41		1.44					0.21				2.06
O4	0.38			1.40				0.20					1.98
O5	1.83				0.20								2.03
O6	1.81												1.81
O7		1.83											1.83
O8		1.78											1.96
OH1	0.59	0.57			0.80								1.96
OH2	0.57	0.59				0.82							1.98
OW1		0.39					0.77	0.80					1.96
OW2	0.40								0.79	0.86			2.05
OW3							0.23				0.81	0.86	1.90
C1				1.11									
C2			1.11										
Σ	6.00	5.97	3.91	3.95	1.00	1.00	1.00	1.00	1.00	1.00	1.00	1.00	

*Bond-valence parameters are from Gagné and Hawthorne (2015). H⁺-O bond valence is based on the graphical relation from Brown (2002).

Mineralogical Magazine and are available as Supplementary material (see below).

Descriptions of the structures

In the uroxite structure, there are two U, two C, 13 O sites (including two OH and three H₂O sites) and eight H sites. Both U atoms in the structure of uroxite are surrounded by seven O atoms forming a UO₇ pentagonal bipyramid. This is the most typical coordination for U⁶⁺ in the solid state, where the two short apical bonds of the bipyramid constitute the UO₂ uranyl group (Burns *et al.*, 1997; Burns, 2005). Two carbon atoms and four equatorial O atoms (O_{eq}: O1, O2, O3 and O4) of the UO₇ bipyramids form oxalate groups. The basic connectivity of cation polyhedra is *via* sharing of two OH vertices (OH1 and OH2) of each bipyramid with other two UO₇ bipyramids; this results in a tetrameric fundamental building block (FBB), [U₄O₂₄]. Oxalate groups connect one tetrameric FBB to four others to form corrugated layers parallel to {102} (Fig. 6). There are two distinct types of ring linkages in the structure of uroxite, four-membered rings (U-OH)₄ creating an unoccupied diamond-shaped void and a much larger eight-membered ring (U-OH-U-Ox)₄, in which uranium atoms are alternately connected by OH and oxalate groups (Fig. 7). These large voids are occupied by the OW3 H₂O groups that are linked strongly by hydrogen bonds to the uranyl oxalate network (Table 6). Adjacent sheets of U polyhedra are linked only *via* hydrogen bonds (Table 6; Fig. 7) and there are no interlayer atoms, resulting in a rather

Table 11. Bond-valence analysis for metauroxite. Values are expressed in valence units.*

	U1	C	H5	H6a	H6b	Σ
O1	1.87					1.87
O2	1.68		0.15			1.83
O3	0.43	1.41			0.17	2.01
O4	0.42	1.45				1.87
OH5	0.54, 0.47		-0.15	0.22		1.08
OW6	0.49			-0.22	-0.17	0.10
C2		0.90				
Σ	5.90	3.76				

*Bond-valence parameters are from Gagné and Hawthorne (2015). Hydrogen-bond strengths are based on O-O bond lengths from Ferraris and Ivaldi (1988).

short spacing of adjacent sheets, as seen by the (102) powder X-ray diffraction line of 4.424 Å (Table 3).

The metauroxite structure has one U, one C and six O sites (including one OH and one H₂O site). As in the structure of uroxite, the U atom is surrounded by seven O atoms forming a squat UO₇ pentagonal bipyramid, with the two short apical bonds of the bipyramid (O_{ap}: O1 and O2) constituting the UO₂ uranyl group. The carbon atom and two equatorial O atoms (O_{eq}: O3 and O4) of the UO₇ bipyramids form C₂O₄ oxalate groups. Two equivalent UO₇ bipyramids share an equatorial OH-OH edge to form a dimer. Oxalate groups connect adjacent uranyl dimers to form chains along [101]. Uranyl oxalate chains are linked to one another only *via* hydrogen bonds (Fig. 8).

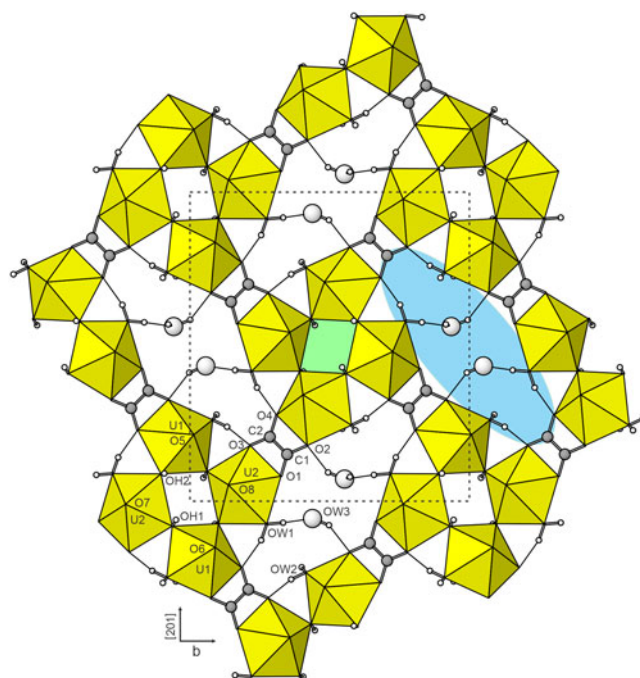


Fig. 6. The layer in the structure of uroxite viewed perpendicular to the {102} sheets. Hydrogen bonds are shown as slender black lines. The unit cell outline is shown by dashed lines. Two coloured areas highlight voids at the centres of two different types of ring linkages: the small vacant area (lime green) built by tetramers of UO₇ polyhedra and the large area (sky blue) formed by four pairs of UO₇ polyhedra alternating with four oxalate groups. Each large area accommodates two OW3 groups.

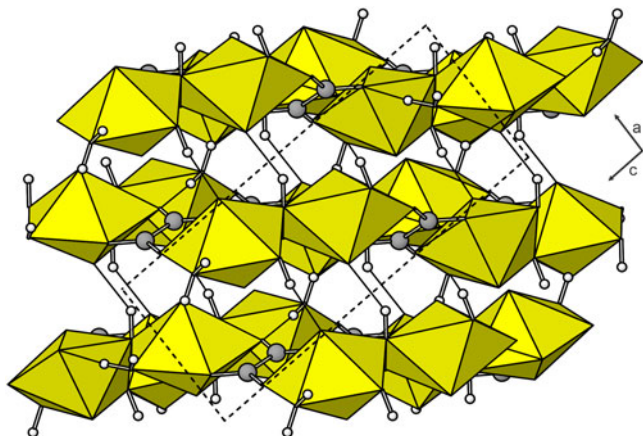


Fig. 7. Stacking of $[(UO_2)_2(C_2O_4)(OH)_2(H_2O)_2]$ sheets (parallel to $[102]$) in the structure of uroxite. The OW3 groups are omitted. The sheets are seen to be linked to one another by hydrogen bonds (single black lines). The unit cell outline is shown by dashed lines.

The C_2O_4 groups link the UO_7 bipyramids in the same way in the structures of both uroxite and metauroxite; however, the UO_7 bipyramids link to one another in quite different ways in the two structures. In the structure of uroxite, each UO_7 bipyramid shares two equatorial OH corners with two other UO_7 bipyramids, resulting in a corner-linked uranyl tetramer, instead of the edge-linked dimer in metauroxite. The quite different structural topologies suggest that it is unlikely that the structures convert from

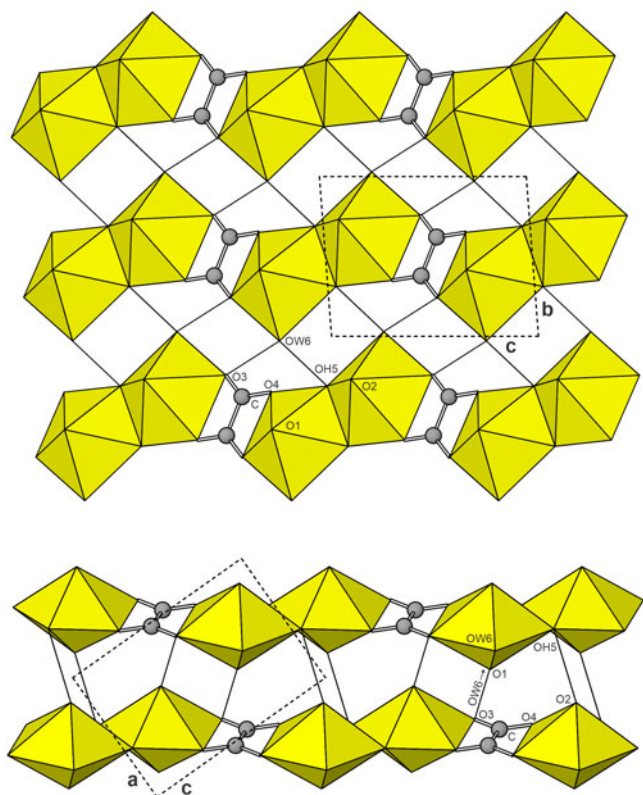


Fig. 8. The structure of metauroxite viewed along $[100]$ (top) and $[010]$ (bottom). Hydrogen bonds are shown with single solid black lines. Note that the hydrogen bond that appears to be between O1 and O3 actually is from an OW6 in a chain behind the one shown. The unit-cell outline is shown by dashed lines.

one to the other. In fact, their close association on some specimens indicates that they form under similar conditions, more or less contemporaneously.

Discussion

The extensive body of research on the synthesis, structural characterisation and properties of actinide oxalates has been driven by the selective affinity of the oxalate group for the actinides in their various oxidation states and, as a consequence, by the wide-ranging assortment of important applications including (but not limited to) radioactive waste management, selective actinide separation and recovery, nuclear fuel recycling and actinide isotope production (*cf.* Abraham *et al.*, 2014). Given the pronounced affinity of oxalate for uranyl cations and the intimate association of uranium mineralisation and carbonaceous plant material in the uranium deposits of the Colorado Plateau, it seems surprising that naturally occurring uranyl oxalates have not been discovered until now. There are two likely reasons: (1) the oxalate group is quite ephemeral in natural systems; its presence in the fossilised carbonaceous plant material would require it to have been quite recently generated and probably only locally in very small amounts; (2) most syntheses of actinide oxalates reported in the literature have utilised conditions quite different from those currently prevailing in the Colorado–Plateau uranium deposits.

As an example of the latter, Duviol *et al.* (2005) synthesised the equivalent of uroxite using $(UO_2)(NO_3)_2 \cdot 6H_2O$, KNO_3 , oxalic acid and water, maintained at $120^\circ C$ for four days. They synthesised the equivalent of metauroxite using U_3O_8 , oxalic acid and water, maintained at $190^\circ C$ for two weeks under autogenous pressure.

At both the Burro and Markey mines, it is likely that the oxalate, $C_2O_4^{2-}$, was derived from the asphaltum matrix (probably fossilised wood), while the uranyl, UO_2^{2+} , was derived from earlier-formed primary (*esp.* uraninite) and/or secondary uranium-bearing minerals. Based upon secondary minerals associated intimately with uroxite and metauroxite and presumably contemporaneously formed, additional cations and anions were also present in the solutions: Na^+ , Ca^{2+} and SO_4^{2-} at the Markey mine and K^+ , Ca^{2+} , SO_4^{2-} , AsO_4^{3-} and VO_4^{3-} at the Burro mine. It is also clear from the modes of occurrence in post-mining secondary assemblages that these minerals formed under ambient conditions: atmospheric pressure, moderate relative humidity and temperatures probably not exceeding $30^\circ C$.

Acknowledgements. Structures Editor Peter Leverett and an anonymous reviewer are thanked for their constructive comments on the manuscript. A portion of this study was funded by the John Jago Trelawney Endowment to the Mineral Sciences Department of the Natural History Museum of Los Angeles County. JP acknowledges support through project GACR 17-09161S of the Czech Science Foundation.

Supplementary material. To view supplementary material for this article, please visit <https://doi.org/10.1180/mgm.2019.57>.

References

- Abraham F., Arab-Chapelet B., Rivenet M., Tamain C. and Grandjean S. (2014) Actinide oxalates, solid state structures and applications. *Coordination Chemistry Reviews*, **266**, 28–68.
- Bartlett J.R. and Cooney R.P. (1989) On the determination of uranium-oxygen bond lengths in dioxouranium(VI) compounds by Raman spectroscopy. *Journal of Molecular Structure*, **193**, 295–300.
- Brown I.D. (2002) *The Chemical Bond in Inorganic Chemistry. The Bond Valence Model*. Oxford University Press, Oxford.

- Burla M. C., Caliandro R., Camalli M., Carrozzini B., Cascarano G.L., Giacovazzo C., Mallamo M., Mazzone A., Polidori G. and Spagna R. (2012) SIR2011: a new package for crystal structure determination and refinement. *Journal of Applied Crystallography*, **45**, 357–361.
- Burns P.C. (2005) U⁶⁺ minerals and inorganic compounds: insights into an expanded structural hierarchy of crystal structures. *The Canadian Mineralogist*, **43**, 1839–1894.
- Burns P.C., Ewing R.C. and Hawthorne F.C. (1997) The crystal chemistry of hexavalent uranium: polyhedron geometries, bond-valence parameters, and polymerization of polyhedra. *The Canadian Mineralogist*, **35**, 1551–1570.
- Carter W.D. and Gualtieri J.L. (1965) Geology and uranium–vanadium deposits of the La Sal quadrangle, San Juan County, Utah, and Montrose County, Colorado. *United States Geological Survey Professional Paper*, **508**.
- Čejka J. (1999) Infrared and thermal analysis of the uranyl minerals. Pp. 521–622 in: *Uranium: Mineralogy, Geochemistry, and the Environment* (P.C. Burns and R. Finch, editors). Reviews in Mineralogy, 38. Mineralogical Society of America, Washington, DC.
- Chenoweth W.L. (1993) The Geology and Production History of the Uranium Deposits in the White Canyon Mining District, San Juan County, Utah. *Utah Geological Survey Miscellaneous Publication*, 93–3.
- Colmenero F. (2019) Structural, spectroscopic, and thermodynamic characterization of ammonium oxalate monohydrate mineral using theoretical solid-state methods. *Journal of Physics and Chemistry of Solids*, **125**, 31–42.
- Duvieubourg L., Nowogrocki G., Abraham F. and Grandjean S. (2005) Hydrothermal synthesis and crystal structures of new uranyl oxalate hydroxides: α - and β -[(UO₂)₂(C₂O₄)(OH)₂(H₂O)₂] and [(UO₂)₂(C₂O₄)(OH)₂(H₂O)₂]-H₂O. *Journal of Solid State Chemistry*, **178**, 3437–3444.
- Ferraris G. and Ivaldi G. (1988) Bond valence vs. bond length in O···O hydrogen bonds. *Acta Crystallographica*, **B44**, 341–344.
- Gagné O.C. and Hawthorne F.C. (2015) Comprehensive derivation of bond-valence parameters for ion pairs involving oxygen. *Acta Crystallographica*, **B71**, 562–578.
- Giesting P.A., Porter N.J. and Burns P.C. (2006). Uranyl oxalate hydrates: structures and IR spectra. *Zeitschrift für Kristallographie – Crystalline Materials*, **221**, 252–259.
- Higashi T. (2001) *ABSCOR*. Rigaku Corporation, Tokyo.
- Kampf A.R., Plášil J., Kasatkin A.V., Marty J. and Čejka J. (2017) Klaprothite, pēligotite and ottohahnite, three new sodium uranyl sulfate minerals with bidentate UO₇–SO₄ linkages from the Blue Lizard mine, San Juan County, Utah, USA. *Mineralogical Magazine*, **81**, 753–779.
- Kampf A.R., Plášil J., Nash B.P., Nēmec I. and Marty J. (2018) Uroxite, IMA 2018-100. CNMNC Newsletter No. 46, December 2018, page 1376; *Mineralogical Magazine*, **82**, 1369–1379.
- Kampf A.R., Plášil J., Nash B.P. and Marty J. (2019) Metauroxite, IMA 2019-030. CNMNC Newsletter No. 50; *Mineralogical Magazine*, **83**, 615–620, doi: 10.1180/mgm.2019.46
- Libowitzky E. (1999) Correlation of O–H stretching frequencies and O–H···O hydrogen bond lengths in minerals. *Monatshefte für Chemie*, **130**, 1047–1059.
- Loiseau T., Mihalcea I., Henry N. and Volklinger C. (2014) The crystal chemistry of uranium carboxylates. *Coordination Chemistry Reviews*, **266**, 69–109.
- Mancilla N., D'Antonio M.C., González-Baróc A.C. and Baranc E.J. (2009) Vibrational spectra of lead(II) oxalate. *Journal of Raman spectroscopy*, **40**, 2050–2052.
- Mandarino J.A. (1981) The Gladstone–Dale relationship – Part IV: The compatibility concept and its application. *The Canadian Mineralogist*, **19**, 441–550.
- Pēligot E. (1942) Recherches sur l'uranium. *Annales de chimie et de physique*, **5** (5), 5–51.
- Peterson K.I. and Pullman D.P. (2016) Determining the structure of oxalate anion using infrared and Raman spectroscopy coupled with Gaussian calculations. *Journal of Chemical Education*, **93**, 1130–1133.
- Pouchou J.-L., and Pichoir F. (1991) Quantitative analysis of homogeneous or stratified microvolumes applying the model “PAP.” Pp. 3l–75 in: *Electron Probe Quantitation* (K.F.J. Heinrich and D.E. Newbury, editors). Plenum Press, New York.
- Shawe D.R. (2011) Uranium–vanadium deposits of the Slick Rock district, Colorado. *United States Geological Survey Professional Paper*, **576-F**.
- Sheldrick G.M. (2015) Crystal Structure refinement with *SHELX*. *Acta Crystallographica*, **C71**, 3–8.
- Shippey T.A. (1980) Vibrational studies of calcium oxalate monohydrate (whewellite) and an anhydrous phase of calcium oxalate. *Journal of Molecular Structure*, **63**, 157–166.